International Symposium on the Conservation of Monuments in the Mediterranean Basin

(2024)

Proceedings of the 11th MONUBASIN (2024)

Numerical evaluation of thermal load applied by magnetic induction and solar loading aimed at experimental analyses using thermo-graphic techniques

Stefano Perilli, Yinuo Ding, Hai Zhang, Stefano Sfarra

doi: 10.12681/monubasin.8317

Numerical evaluation of thermal load applied by magnetic induction and solar loading aimed at experimental analyses using thermographic techniques

Stefano Perilli, *Department of Information Engineering, Electronics and Telecommunications*, "Sapienza" University of Rome
stefano.perilli@uniroma1.it

Yinuo Ding, *Centre for Composite Materials and Structures (CCMS)*, Harbin Institute of Technology, 150001, Harbin, China
dyndeyx@163.com

Hai Zhang, *Centre for Composite Materials and Structures (CCMS)*, Harbin Institute of Technology, 150001, Harbin, China
hai.zhang@hit.edu.cn

Stefano Sfarra, *Department of Industrial and Information Engineering and Economics*, University of L'Aquila, 67100, L'Aquila, Italy
stefano.sfarra@univaq.it

Abstract. The study describes a first approach of integration among infrared thermography inspections under solar loading conditions, and a heating provided by magnetic induction in view of a future induction thermography test. An ancient bronze helmet, part of a statue located in L'Aquila (Italy) and inaugurated on *October 14th, 1928*, is the sample under test *(SUT)* herein. The corrosion process over time (17 years: 2007 – 2024) is evaluated via numerical and experimental techniques. It requires the presence of a temperature gradient priming the heat transfer mechanism through the *SUT*. Experimental configurations of infrared thermography (*IRT*) allowed the detection of defects like *e.g.* cracks and pitting. For this reason, the study was integrated with a preliminary magnetic induction test, *i.e.* a numerical model, in view of a future *in situ* thermographic test. To determine the appropriate distance and working time of the induction heater, a modelling was carried out in *COMSOL Multiphysics*®. The ancient bronze helmet was acquired by a non-contact instrument produced by *CREAFORM model Go! SCAN 3D*®. The mesh was exported in *COMSOL Multiphysics*® for further conditioning and processing. In particular, the authors used the *magnetic field coupling with a heat transfer* package to obtain a reasonable thermal distribution on the modeled artefact. Concerning the thermographic analyses, a *FLIR S65 HS* and a *FLIR T1020* thermal camera were used in the *2007* and *2024* inspections, respectively. A preliminary post-processing of the latest thermographic data is performed herein.

Keywords: Solar loading, Infrared thermography, Numerical modelling with *magnetic field coupling with heat transfer*, Laser scanner geometric reconstruction, Bronze.

1 Introduction

The evolution of climatic phenomena over the centuries due to the natural course of events and environmental changes has led to significant corrosion problems in bronze artifacts. This involves the variation of both the chemical composition and the aesthetic appearance. The surface of bronze and copper monuments is increasingly exposed to products of crystalline corrosion, *e.g.* copper oxide (cuprite) and basic copper sulphates. In urban areas, there is an increase in the formation of copper sulphates, which leads to byproducts. The discoloration/degradation of metal surfaces is caused by acid deposition, which usually results in extensive pitting that first affects the surface layer and then penetrates deeply, resulting in profound and irreversible alterations. In this regard, the passive thermography approach integrated with numerical modelling turns out to be an excellent solution allowing the analysis of the corrosion effect [1], [2] by studying the thermal contrast generated between defective and sound areas [3-7]. An inductive

heater was numerically modelled in our work; thereafter, the main technical parameters were inversely retrieved to obtain on the SUT the same thermal contrast initially generated by the solar loading.

2 Methodology

In 2007, an ancient bronze helmet shown in Fig. 1 was thermographically inspected using a *FLIR S65 HS* thermal camera [5]; the thermal field allowed the evaluation of the corrosion level thanks to an *ad hoc MATLAB®* script [6]. Thermographic measurements were repeated in 2024 using a new thermal camera. Fig. 1 summarizes the logical process followed in this work.

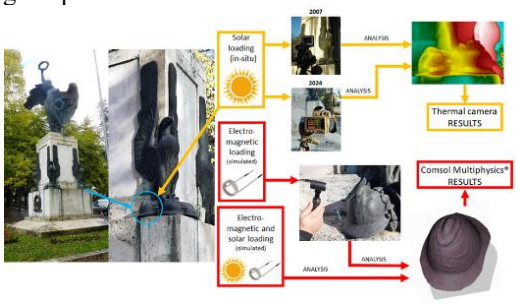

Fig. 1. Key steps followed during the numerical-experimental evaluation performed on the ancient bronze helmet.

To analyze the same helmet through numerical simulations, its geometry was recorded via *CREAFORM model Go! SCAN 3D®*. The geometry shows a rather regular pattern. However, for 3D laser scanners, the dark-green color is probably the most difficult to acquire. Usually, circular "spot" stickers are applied to the objects to form an ordered sequence of fiducials on the geometry that helps the software during the triangulation and reconstruction phases of the surface. Since the artefact is an ancient object, it hasn't been possible to apply this procedure. Furthermore, since the surface is particularly pitted – *i.e.*, a typical effect of surface corrosion -, the recording phase was further complicated; even denser point clouds were needed to guarantee detailed acquisitions in the order of a *tenth* of a *mm*. However, an initial correction of the individual point clouds was carried out. The main steps, explained in the following, are summarized in Fig. 2. The *RevoScan5®* computer program was used in our case (Fig. 2a).

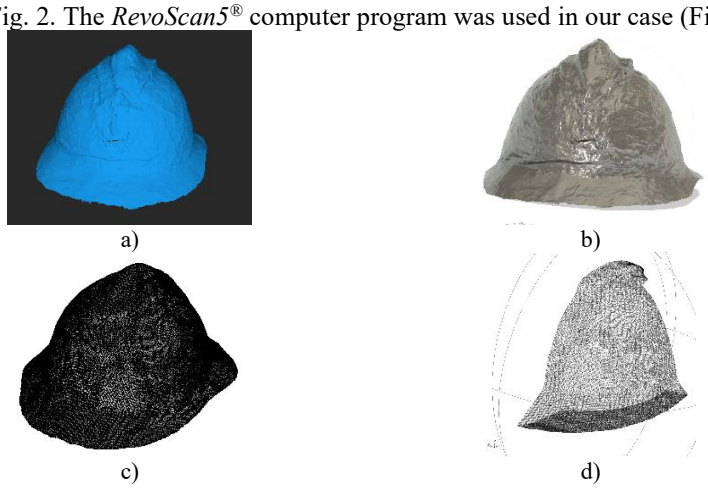

Fig. 2. Reconstruction of the geometry until the mesh; a) point cloud obtained by *RevoScan5®*; b) solid geometry via *Autodesk® Fusion® 360*; c) complete mesh obtained in *COMSOL Multiphysics®*; d) mesh analyzed in *COMSOL Multiphysics®*.

The file includes *1725426* vertices and *3442241* polygons. Given the considerable size and computational cost, it was necessary to process the point cloud using *Autodesk® PowerShape®* software; the holes were filled, and the tangent polygonal elements were regularized. The point cloud, being a surface without thickness, requires further processing to make it a solid. The reconstruction, shown in Fig. 2b, was carried out with *Autodesk® Fusion® 360.* A final solid useful for the numerical modelling in *COMSOL Multiphysics®* was finally obtained. Readers should note that the model in Fig. 2c is filled with material. However, the helmet has a non-constant thickness; it was emptied using another mesh. The reason for this step is the stability of the *.IGES* format compared to *.stl* format. Given the high computational cost

of this model - *i.e.*, *4139342* nodal elements - it needs a motherboard with a *RAM* greater than *128 GB* [8]. For this reason, it was necessary to carry out a volumetric/nodal reduction of the model by exploiting the real location of the helmet that has the rear part attached to the base of the statue, while the right and left sides are approximately a plane of symmetry. A model reduction was operated (Fig. 2d), obtaining *220932* volume elements, *76686* surface elements, *73526* sides with *450595* external degrees of freedom, and *566702* internal degrees of freedom. This geometry was processed with a *12th Gen Intel(R) Core (TM) i9-12900H 2.50 GHz, RAM 32,0 GB, 14 Cores*.

3 Experimental results

As previously mentioned, the same helmet was inspected again in 2024 into the long-wave infrared spectrum (LWIR); the thermal field was initially acquired, and subsequently the corrosion areas detected using *MATLAB®*. Numerical modelling was built for thermal contrast purposes. Tab. 1 summarizes the main thermophysical parameters used in our numerical model.

Table 1. Bronze: main thermophysical parameters.

C_p Specific heat at constant pressure *[kJ/kgK]*	**0.4** [9]
ρ Density *[kg/m³]*	**8.8·10³** [9]
k Thermal conductivity *[W/mK]*	**50** [10]
ε Emissivity	**0.55** [5]

The heat transfer mechanism was based on the following governing equations set:

$$\rho C_p \frac{\partial T}{\partial t} + \rho C_p \boldsymbol{u} \cdot \nabla T + \nabla \cdot \boldsymbol{q} = Q + Q_p + Q_{vd} \quad (1)$$

$$\boldsymbol{q} = -k\nabla T \quad (2)$$

$$J = \varepsilon e_b(T) FEP_i(T) + \rho_d G \quad (3)$$

$$e_b(T) = n^2 \sigma T^4 \quad (4)$$

where ρ is density *[kg/m³]*, C_p specific heat at constant pressure *[J/kgK]*, $\boldsymbol{u}$ velocity vector air flux *[m/s]*, T temperature *[K]*, t is time *[s]*, $\boldsymbol{q}$ thermal flux vector evaluated by Fourier law for heat transfer via conduction, Q source/sink of heat *[W/m³]*, Q_{vd} viscous heat dissipation sink *[W/m³]*, Q_p point heat source *[W/m³]*, k thermal conductivity for complete materials *[W/mK]*, J total incoming radiative flux, FEP_i view factor linked to the relative sun-SUT position (it also includes the fractional emissive power of the blackbody), ε emissivity *[%]*, $e_b(T)$ power radiated across all wavelengths depending on the 4th power of temperature. The latter varies instantly and is responsible for the increase or decrease in irradiance (G) *[W/m²]* throughout the day; σ represents the Stefan-Boltzmann constant. The numerical model works with the real irradiance. The environmental parameters inherent to the closer weather station to the SUT were provided by CETEMPS (L'Aquila, Italy) and shown in Tab.2.

Table 2. Main environmental parameters recorded by a weather station.

Time	Air temperature *[K]*	Solar irradiance *[W/m²]*	Wind speed *[m/s]*	RH *[%]*
7:00 AM	**271.22**	**173.8**	**0.56**	**81.8**
8:00 AM	**275.68**	**355.87**	**0.22**	**68.87**
9:00 AM	**278.98**	**474.6**	**0.15**	**57.16**

Concerning the model of the solar loading, the orientation of the mesh towards the relative *x,y,z* axes (related to the absolute reference axes of the geographical orientation) was fundamental. The geographic coordinates provided to the model were: *42.345151, 13.397797*. In this case, the authors used the natural convection and RH values reported in Tab. 2. The *GMRES* solver coupled with the *MULTIGRID* function was implemented and applied to the data. A frame rate of five minutes during two hours of inspection (from 7:00 AM) was selected. As shown in the modelling inherent to the different time intervals (Fig. 3a), the bronze material, as a whole, has a good thermal contrast. The helmet, that is at thermal equilibrium with the ambient temperature (Tab. 1) before dawn, is fully affected by a low solar load, operating a heat flux reaching the maximum depth; it is particularly noticeable starting from 90th minute (Fig. 3a).

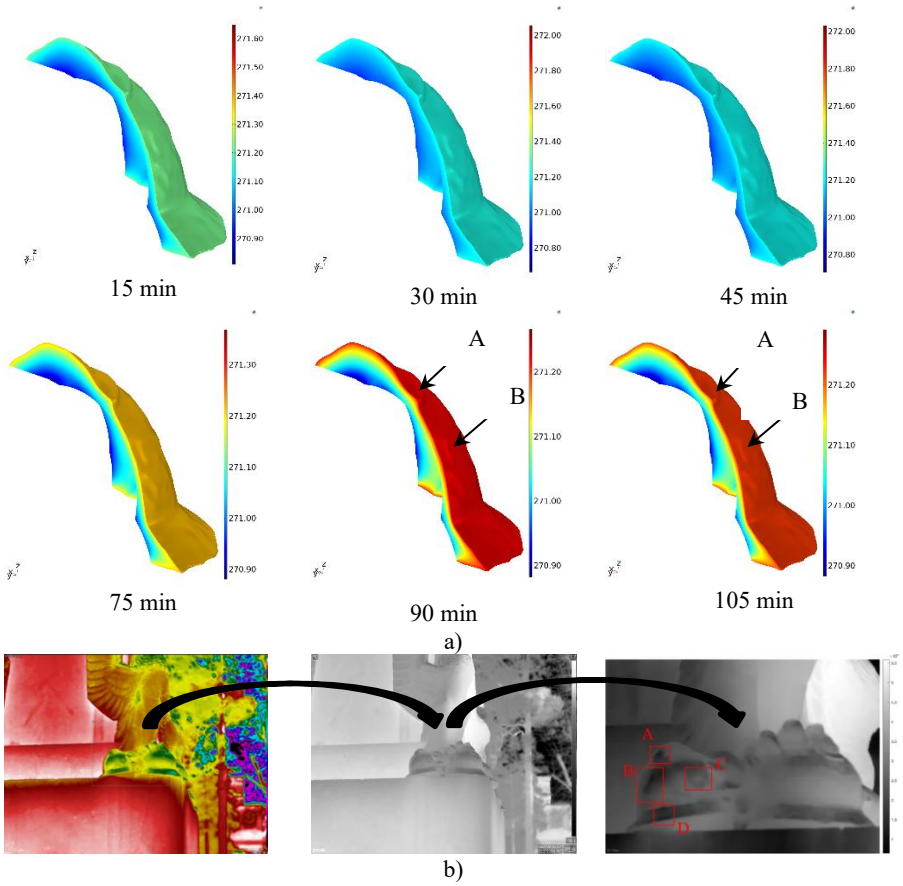

Fig. 3: a) Numerical simulation of the helmet showing the external and internal thermal fields along a selected cross-section: frame rate of 15 min, multiplying by three as was done during the 2007 thermographic test; b) Conversion of the RGB images into single-channel grayscale images, cropping and normalizing procedures of the 2024 thermographic test.

The effect of complete radiation on the SUT is also evident in Fig. 3b, that is related to the 2024 thermographic test. The numerical model approximates the thermal field in a satisfactory way (Fig. 3a), highlighting the slight temperature gradients on the surface. This demonstrates that pitting was computed thanks to local gradients. As evident in Fig. 3a, no shadows on the back of the model are present at the first light of dawn (sunrise starts at 06:45 AM [11]). The increase of solar irradiance and the relative evolution of the thermal field manifest themselves along the depth of the helmet cross-section starting from 90th minute. *A* and *B* defects indicated in Fig. 3a (at 90th and 105th minute) are detectable in Fig. 3b (experimental result), too. Defects *C* and *D* haven't been included in this part of the numerical modelling due to computational reasons.

This step allows defining the correct parameters to be imposed at the magnetic induction heater to obtaining a similar thermal contrast on a small part of the SUT whether compared to the one facing the sun. The working principle of a magnetic induction heater is very different with respect to a common electric resistance. Everything originates from an oscillator, that is an electronic circuit capable of generating waveforms whose amplitude can be modulated. Amplitude modulation, for energy conservation, generates frequency variation. The electric current flowing out of the oscillator is, therefore, frequency-modulated. If this current is allowed to flow through a solenoid, then the coils will generate a circular electric field. If the current is alternating, the electric field and the magnetic field are orthogonal to each other. Therefore, a circular electric field (due to the coils of the inductor) will bring an orthogonal magnetic field to the main axis of the winding. An oscillating current in the solenoid (*i.e.*, a variation in the direction of the electric current vector) leads to an oscillation of the induced magnetic field (*i.e.*, a variation in the direction of the magnetic field vector). This effect excites the particles of the material to be heated, causing the spin of the electrons of which the matter is made to continuously change. This continuous change generates a *Joule effect* that causes the thermal load in the material under inspection.

The *Beta 1852 R* heater designed for this application has a 50Hz fixed frequency circuit, therefore, to vary the heating effect the user can act only to the working time or distance between the coil and the

component. This choice was dictated to generalize the experiment, allowing application also through common and non-dedicated equipment.
Given the high computational cost that would arise in *COMSOL Multiphysics®* for coupling *Heat transfer in solid* and *Magnetic field* functions, a separate numerical model was adopted for such a large mesh. The aim was to evaluate the thermal imprint released on a flat bronze plate considering a frequency of 50Hz by varying only the working time and the heater-sample distance. The governing equations of the modelling are the following [12]:

$$E = -j\omega A \quad (5)$$

$$\nabla \times \boldsymbol{H} = \boldsymbol{J} \quad (6)$$

$$\boldsymbol{B} = \nabla \times \boldsymbol{A} \quad (7)$$

$$\boldsymbol{J} = \sigma \boldsymbol{E} + j\omega \boldsymbol{D} \quad (8)$$

With $\boldsymbol{E}$ electric field *[V/m]*, ω angular frequency *[rad/s]*, $\boldsymbol{J}$ current density volume *[A/m²]*, $\boldsymbol{H}$ magnetic field *[A/m]*, $\boldsymbol{B}$ magnetic flux density *[T]*, $\boldsymbol{A}$ magnetic potential (vector) *[Wb/m]*, σ electrical conductivity, and $\boldsymbol{D}$ electric displacement or electric flux density *[C/m²]*.
Fig. 4a) shows the model generating information vectors used in the final modelling. The coupling of these two models allowed us to obtain the thermal behavior occurring at a 10 mm distance between the solenoid and the SUT at different times (see Figs. 4b), c), d), e), and f)).
The choice of 10 mm distance was dictated by a series of numerical tests; it was assessed that for shorter distances, the heating effect is too sudden, *i.e.* in the order of hundredths of a second, while for greater distances, the bronze is affected by a very slow magnetic field. Figs. 4 b), c), d), e), and f) also show how the user has the possibility of choosing the working time to obtain an appropriate thermal contrast for the *in situ* thermographic measurements. The authors will consider equipping the electrical connection of the heater to a programmable time switch to control the evolution of the thermal imprint; this is the future perspective of the present work.

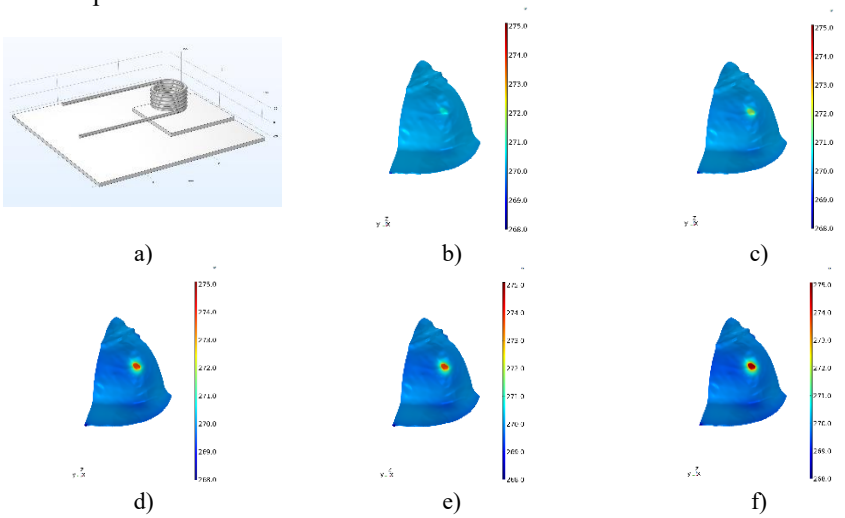

Fig. 4. Numerical model of the magnetic analysis coupled with *heat transfer in solid* and subsequent application of the coupling results to the original model for the study of the local thermal contrast: a) modelling of the active inductor for the study of the imposed thermal contrast; b) local effect of the heater on the bronze helmet using a magnetic inductor working for 0.2 s; c) 0.4 s; d) 0.6 s; e) 0.8 s; and f) 1 s.

4 Conclusions

In this work, thermal imprints retrieved in an ancient helmet via a complex numerical analysis involving the use of an advanced 3D laser scanner were evaluated by setting thermophysical parameters and boundary conditions inherent to specific years.
In the years 2007 and 2024, thermal images were indeed recorded and their comparison helped to understand the evolution over time of the corrosion process.
With a view to a future thermographic inspection aimed at analyzing with greater detail the corrosion in the helmet, it was considered of interest to evaluate whether the thermal load, usually provided by the passive thermography approach in artworks facing the sun, could be replaced by an equivalent one given by an inductive heater. The analysis led to satisfactory results, allowing the obtaining of appropriate

thermal imprints using a commercial and non-dedicated inductive heater, leaving the probe working time as the only parameter to be controlled.
In the future, an *in-situ* induction thermography analysis supported by such a numerical procedure will be performed to validate our preliminary results.

Acknowledgements
The authors are grateful to CETEMPS—Center of Excellence in Telesensing of Environment and Model Prediction of Severe events (L'Aquila, Italy) for providing the data recorded by the weather station. The authors would also like to thank Eng. Luigi Berri of AXIST SRL (Rivoli, Italy) for the loan of the 3D scanner, and Eng. Stefano Perilli (University of Rome – La Sapienza, Italy) for the scientific support provided with COMSOL.
This work was supported by the Italian Ministry of University and Research (Grant n. PGR02016 – CUP: E13C24000350001), and the National Key R&D Program of China (Grant No. 2023YEF0197800).

References

1. P.A. Schweitzer, Corrosion of Linings and Coatings: Cathodic and Inhibitor Protection and Corrosion Monitoring**,** Corrosion Engineering Handbook, 2nd Edition, Marcel Dekker, New York (2006).
2. A. Lins and T. Power, "The Corrosion of Bronze Monuments in Polluted Urban Sites: A Report on the Stability of Copper Mineral Species at Different pH Levels", Ancient & Historic METALS – Conservation and scientific research, 119-121 (1991).
3. M.P. Vieira de Souza, F. López, X. Maldague, "Corrosion under insulation mitigation by passive multivariate thermography", Quantitative InfraRed Thermography Journal (2024) DOI: 10.1080/17686733.2024.2305917.
4. B. Oswald-Tranta, A. Hackl, P. Lopez de Uralde Olavera, E. Gorostegui-Colinas & A. Rosell, "Calculating probability of detection of short surface cracks using inductive thermography", Quantitative InfraRed Thermography Journal, Vol. 21, No. 2 (2024), pp. 82-101 DOI: 10.1080/17686733.2022.2152259.
5. D. Ambrosini, A. Paoletti, D. Paoletti, S. Sfarra, "NDT methods in artwork corrosion monitoring", Proceedings of SPIE, (2007), Volume 6618, Article number 661817, O3A Optics for Arts, Architecture and Archaeology, DOI: 10.1117/12.725556.
6. X.P.V. Maldague, "Theory and practice of infrared technology for nondestructive testing", Wiley, New York (2001).
7. G. Washer, R. Fenwick, N. Bolleni "Effects of solar loading on infrared imaging of subsurface features in concrete", Journal of Bridge Engineering, Vol. 15, No. 4 (2010), pp. 384-390 DOI: 10.1061/(ASCE)BE.1943-5592.000011.
8. J. Yström, "Solving Larger Models in COMSOL Multiphysics®", COMSOL webinar, Boston. https://www.comsol.com/video/solving-larger-models-in-comsol-multiphysics. Accessed on 10 April 2024.
9. N. Orazi, "The study of artistic bronzes by infrared thermography: A review", Journal of Cultural Heritage, Vol. 42 (2020), pp. 280-289 DOI: 10.1016/j.culher.2019.08.005.
10. B.J. Monaghan, J.G.J. Neale, L.A. Chapman, "Some thermal properties of a copper-tin alloy", International Journal of Thermophysics, Vol. 20, No. 4 (1999), pp. 1051-1060 DOI: 10.1023/A:1022694518254.
11. http://www.meteoam.it. Accessed on 25 February 2024.
12. J.R. Cardoso, "Electromagnetics through the Finite Element Method – A simplified approach using the Maxwell's Equations", 1st Edition, CRC Press, Boca Raton, (2017) DOI: 10.1201/9781315366777.